

D. Jaksch<sup>1</sup>, C.W. Gardiner<sup>2</sup> and P. Zoller<sup>1</sup>

<sup>1</sup> *Institut für Theoretische Physik, Universität Innsbruck, 6020 Innsbruck, Austria*

<sup>2</sup> *Physics Department, Victoria University, Wellington, New Zealand*

We present results of simulations of a *quantum Boltzmann master equation* (QBME) describing the kinetics of a dilute Bose gas confined in a trapping potential in the regime of Bose condensation. The QBME is the simplest version of a quantum kinetic master equations derived in previous work. We consider two cases of trapping potentials: a 3D square well potential with periodic boundary conditions, and an isotropic harmonic oscillator. We discuss the stationary solutions and relaxation to equilibrium. In particular, we calculate particle distribution functions, fluctuations in the occupation numbers, the time between collisions, and the mean occupation numbers of the one-particle states in the regime of onset of Bose condensation.

## I. INTRODUCTION

In the previous two papers [1,2], which we will refer to as QKI and QKII, a fully quantum mechanical kinetic theory for Bose gases was developed. One of the simplest versions of the quantum kinetic master equation (QKME) neglects all spatial dependence, and yields a master equation, which we have named the quantum Boltzmann master equation (QBME). In contrast to the familiar quantum Boltzmann equation (QBE) [3,4], which is an equation of the single particle distribution function, the QBME is an  $N$ -atom stochastic equation. The aim of the present paper is to present results of numerical simulations of this equation for finite size systems consisting typically of a few hundred atoms. Although the exclusion of the spatial dependence is an extreme simplification, these simulations will give us a first orientation about the kind of solutions the QKME will yield. These simulations can thus serve as a guideline for the type of approximations of the QKME one may use to find numerical solutions of this much more interesting, but unwieldy, equation.

Furthermore, we will concentrate our attention on those results of the QBME which cannot be obtained using equations like the quantum Boltzmann equation (QBE). We also restrict our work to the region of temperatures which are less than or not much higher than the critical temperature of the gas, because at much higher temperatures quantum effects do not play a crucial role and simulations of the classical Boltzmann equation, which is valid in that case, have already been performed [5].

The QBME is a genuine  $N$ -atom equation like the QKME, but it neglects all the coherences contained in the QKME—it is thus intermediate between the QKME

and the description of the system with kinetic equations for single-particle distribution functions. Its irreversibility comes from the Markov assumption employed in deriving the QKME.

The paper is organized as follows. In Sec. II we review the derivation of the QBME in QKI [1], discuss properties of the QBME, and compare it with the QBE. Furthermore, we give a brief description of the simulation algorithm. In Secs. III and IV we apply the QBME to study a Bose gas confined in a 3D box and in a 3D harmonic oscillator. In particular, we discuss simulation results for thermodynamic quantities, the mean time between collisions, and the fluctuations of the occupation numbers of the condensate. For the 3D harmonic oscillator we also simulate a gas that is evaporatively cooled.

## II. THE QUANTUM BOLTZMANN MASTER EQUATION

In this section we will first summarize the derivation of the quantum Boltzmann master equation as given in QKI [1]. Furthermore, we discuss properties of this equation and its solutions which are relevant for our numerical studies presented in Secs. III and IV, and conclude with a comparison of the QBME with the QBE.

### A. Derivation and validity of the QBME

The second quantized form of the Hamilton operator for a Bose gas with pair particle interaction can be written  $H = H_0 + H_I$ , where

$$H_0 = \sum_{\mathbf{m}_i} \hbar\omega_{\mathbf{m}_i} a_{\mathbf{m}_i}^\dagger a_{\mathbf{m}_i}, \quad (1)$$

$$H_I = \frac{1}{2} \sum_{\mathbf{m}_1, \mathbf{m}_2, \mathbf{m}_3, \mathbf{m}_4} U_{\mathbf{m}_1, \mathbf{m}_2, \mathbf{m}_3, \mathbf{m}_4} a_{\mathbf{m}_1}^\dagger a_{\mathbf{m}_2}^\dagger a_{\mathbf{m}_3} a_{\mathbf{m}_4}. \quad (2)$$

Here  $H_0$  is the system Hamilton operator of the non-interacting Bose gas where  $a_{\mathbf{m}_i}^\dagger$  is the creation operator of a particle in the eigenstate of  $H_0$  labeled  $\mathbf{m}_i$  with energy  $\hbar\omega_{\mathbf{m}_i}$ . The trapping potential is included in  $H_0$ .

The interaction Hamiltonian  $H_I$  describes two body interactions in the Bose gas. In the regime we want to study, only  $s$ -wave scattering plays an important role, allowing us to write

$$\begin{aligned}
U_{\mathbf{m}_1, \mathbf{m}_2, \mathbf{m}_3, \mathbf{m}_4} &= \frac{4\pi\hbar^2 a}{m} \int_{R^3} d^3x \Psi_{\mathbf{m}_1}^*(\mathbf{x}) \Psi_{\mathbf{m}_2}^*(\mathbf{x}) \Psi_{\mathbf{m}_3}(\mathbf{x}) \Psi_{\mathbf{m}_4}(\mathbf{x}). \quad (3)
\end{aligned}$$

In Eq. (3)  $\Psi_{\mathbf{m}_i}(\mathbf{x})$  denotes an eigenfunction of the trapping potential in coordinate space labeled by quantum numbers  $i$ . Below we will specify the potential to be a 3D box with periodic boundary conditions (Sec. III), or a 3D isotropic oscillator (Sec. IV), and will give expressions for the matrix elements  $U_{\mathbf{m}_1, \mathbf{m}_2, \mathbf{m}_3, \mathbf{m}_4}$  for these specific cases. For convenience we will use the notation  $i$  instead of  $\mathbf{m}_i$  below. The scattering length of the gas is  $a$  and the mass of the gas particles is  $m$ . We will treat systems with finite number of particles  $N$ . This is the starting point from which the QKME is derived in QKI. The following assumptions and approximations are made:

### 1. The forward scattering terms

All the terms of  $H_I$  (see QKI Eq. (67)) which commute with the system Hamiltonian  $H_0$  describe forward scattering and give rise to the mean field. These terms can be included with  $H_0$ . Forward scattering does not change the occupation of the one-particle eigenstates, so we will neglect the influence of these terms on the eigenstates of  $H$  in the simulations.

### 2. The collision terms

The remaining terms in  $H_I$  describe collisions which change the occupation numbers of the one-particle states of the trapping potential. We assume that this part of  $H_I$  can be treated perturbatively, using the Born approximation and the Markov approximation (QKI Sec. IV C 3). The Born approximation is valid when the interaction between the particles is small compared to the system Hamiltonian  $H_0$  [6]. For the Markov approximation to be valid it is required that the frequency spectrum is effectively continuous which means that the separation between the energy levels is much smaller than the energy range of occupied states. The use of the Markov approximation gives the QKME its irreversible character. We will neglect the influence of collisional shifts on eigenstates of  $H$ .

### 3. Reduction of the QKME to the QBME

To reduce the QKME to the QBME it is assumed that the coherent terms (i.e. Hamiltonian terms in QKI Eq. (77)) can be neglected. The QBME is an equation for the diagonal elements  $w_{\mathbf{n}} \equiv \langle \mathbf{n} | \rho | \mathbf{n} \rangle$  of the density operator and takes the following form (QKI Eq. (101)):

$$\begin{aligned}
\dot{w}_{\mathbf{n}} &= -\frac{\pi}{\hbar} \sum_{1234} \delta(\hbar(\omega_1 + \omega_2 - \omega_3 - \omega_4)) |U_{1234}|^2 \\
&\times \{n_1 n_2 (n_3 + 1) (n_4 + 1) [w_{\mathbf{n}} - w_{\mathbf{n} + \mathbf{e}_{1234}}] \\
&+ (n_1 + 1) (n_2 + 1) n_3 n_4 [w_{\mathbf{n}} - w_{\mathbf{n} - \mathbf{e}_{1234}}]\}. \quad (4)
\end{aligned}$$

Here  $|\mathbf{n}\rangle = |n_0, n_1, n_2, \dots\rangle$  is a Fock state of the  $N$ -particle system, giving the occupation numbers  $n_i$  of the eigenstates  $\Psi_i(\mathbf{x})$  and  $\mathbf{n}$  denotes the vector consisting of the occupation numbers  $n_i$ . The vector  $\mathbf{e}_{1234}$  is defined similarly to  $\mathbf{n}$  as

$$\mathbf{e}_{1234} = [0, \dots, 0, \overset{1}{1}, 0, \dots, 0, \overset{2}{1}, 0, \dots, 0, \overset{3}{-1}, 0, \dots, 0, \overset{4}{-1}, 0, \dots, 0], \quad (5)$$

which describes two particle collisions. The state  $|\mathbf{n} - \mathbf{e}_{1234}\rangle$  can thus be reached from  $|\mathbf{n}\rangle$  by the collision  $1 + 2 \rightarrow 3 + 4$ .

The  $\delta$ -function in the discrete sum of the QBME (4) has its origin in the use of the Markov approximation as outlined in QKI. Since we do not replace these sums by integrals in our simulations this  $\delta$ -function requires interpretation. We concentrate energy regions of  $\Delta e$  to one single discrete energy level. The energy interval is described by the properties of the closest one-particle state of  $H_0$ . The choice of  $\Delta e$  depends on the trapping potential and is such that each of the one-particle states serves as one of the discrete energy levels with energy  $e_i$  that determine the properties of particles within the energy range  $[e_i - \Delta e/2, e_i + \Delta e/2]$ . Implicitly this includes the interpretation of  $n_i$  as being an integral over a smooth distribution function  $f(e)$ :

$$n_i = \int_{e_i - \Delta e/2}^{e_i + \Delta e/2} de \frac{f(e)}{\Delta e} \quad (6)$$

where  $f(e)$  gives the number of particles occupying a state with energy  $e$ . Among the degenerate one-particle eigenstates the particles are distributed according to similar arguments as in Eq. (6). The  $\delta$ -function in the QBME (4) has, therefore, to be interpreted as

$$\delta(e) = \frac{\delta_{e,0}}{\Delta e} \quad (7)$$

and  $w_{\mathbf{n}}$  in the QBME (4) is the probability of finding  $n_i$  particles within the energy interval  $[e_i - \Delta e/2, e_i + \Delta e/2]$ .  $\delta_{x,y}$  denotes the Kronecker delta.

In QKI it is shown that the kernel of the integral where the Markov approximation is made (QKI Eq. (68)) has a width given by the temperature  $\hbar/kT$ . This width determines the range of possible outcomes of a

collision. As long as  $\hbar/kT$  is much smaller than the time between two collisions the free evolution after the kernel has reached zero will fix the energy of the particles within a range of  $\hbar/t_{\text{coll}}$  before the next collision occurs. We already assumed that it is possible to describe the system in terms of one-particle eigenstates of the trapping potential which is only valid if the level broadening coming from the collisions is much less than the level

spacing. Hence, we are able to decide which of our one-particle states describes the properties of a particle best before this particle collides again.

#### 4. Discussion

Since there are no classical assumptions in deriving the QBME (4), it should be valid even when the Bose gas becomes degenerate, within the limits of the approximations made in its derivation. The quantum statistics is contained in the  $1 + n_i$  factors in Eq. (4). This allows us to study the onset of BEC, in the sense of obtaining a macroscopic occupation in the ground state [7], and in particular finite number effects which are important when the number of atoms is not large.

The QBME (4) is a full  $N$ -particle equation in the form of a stochastic master equation which describes  $N$  particles interacting with each other by two particle collisions. These collisions are responsible for the equilibration process. In contrast, the QBE (see Sec. IID) considers the motion of one particle interacting with a mean distribution of the other atoms in the gas.

No mean field effects are included in the present form of the QBME (4). As soon as the temperature  $T$  of the gas is far below the critical temperature  $T_c$  and most of the particles have accumulated in the ground state, the mean field produced by these condensed particles must be taken into account. Furthermore, the derivation of the QBME assumes that the width of the energy levels and collisional shift in addition to the mean field is small relative to the level spacing  $\Delta e$ .

### B. Quantities of interest

For comparison with the simulations discussed in the following sections, we summarize below properties of the stationary solutions, the particle distributions and collision times.

#### 1. Stationary solution

The QBME conserves energy  $E$  and number of particles  $N$ . According to QKI the stationary solution of the QBME (4) is

$$w_{\mathbf{n}} = \text{constant}, \quad (8)$$

corresponding to a microcanonical ensemble.

We will also compare our simulations results with the grand canonical ensemble. For the mean occupation numbers one obtains (compare QKI Sec. V A 2)

$$\langle n_i \rangle = \frac{1}{\exp\left(\frac{\hbar\omega_i - \mu}{kT}\right) - 1}. \quad (9)$$

In this case  $T$  is the temperature and  $\mu$  is the chemical potential of the system in the grand canonical ensemble. Given the mean energy of the system  $E$  and the mean number of particles  $N$  we can solve the two equations

$$N = \sum_i \frac{1}{\exp\left(\frac{\hbar\omega_i - \mu}{kT}\right) - 1} \quad (10a)$$

$$E = \sum_i \frac{\hbar\omega_i}{\exp\left(\frac{\hbar\omega_i - \mu}{kT}\right) - 1} \quad (10b)$$

for  $\mu$  and  $T$  numerically. We will compare this result below with the one we get from our simulations. In the framework of the QBME these grand canonical results are obtained if we assume that in steady state the expectation values of the  $n_i$  factorize (which is an approximation).

#### 2. Particle distributions

The QBME is a stochastic equation for the diagonal elements of the density operator in the basis of the eigenstates of  $H_0$ . We are interested in calculating the probability distribution of particles in the one-particle states. They are defined as

$$W_i(j) = \sum_{\substack{\mathbf{n} \\ n_i=j}} w_{\mathbf{n}}, \quad (11)$$

and give the probability of finding  $j$  particles in the one-particle eigenstate labeled  $i$ . The sum runs over all  $\mathbf{n}$  with  $\sum_i n_i = N$  and  $\hbar \sum_i \omega_i n_i = E$ , the constant number of particles in the gas and the energy of the system, respectively. We will compute these distributions for the 3D box in Sec. IIIB 4.

For highly excited states  $i$ , whose mean occupation number is much less than 1 the probability  $W_i(j)$  is only substantially different from zero for  $j = 0$  and  $j = 1$ , which leads to  $\langle n_i^2 \rangle - \langle n_i \rangle^2 \approx \langle n_i \rangle$ . On the other hand, approximate expressions can be derived for low lying states, including the ground state, on the following arguments. Assuming that there is no restriction on how the particles are distributed among degenerate energy levels we can write  $W_i(j)$  in terms of energy levels [8]

$$W_{\bar{i}}(j) = \frac{1}{Z} \sum_{\bar{n}} \prod_{\bar{l}} \frac{(g_{\bar{l}} n_{\bar{l}} + g_{\bar{l}} - 1)!}{(g_{\bar{l}} n_{\bar{l}})! (g_{\bar{l}} - 1)!}. \quad (12)$$

Here  $\bar{l}$  are sets of indices of degenerate eigenlevels,  $g_{\bar{l}}$  is the number of elements of  $\bar{l}$ , and  $g_{\bar{l}} n_{\bar{l}}$  gives the total number of particles in the states  $l \in \bar{l}$ . The normalization constant is denoted by  $Z$ , and  $\bar{n}$  is a vector containing the  $n_{\bar{i}}$ . This formula is only approximate because it includes configurations of the system that cannot occur in the simulations since they are not connected by collisions with the initial configuration. For small temperatures the sum in Eq. (12) is readily calculated numerically, and we will compare this with our simulation results in Sec. IIIB 4.

For any given configuration  $\mathbf{n}$  of the system we calculate the sum over all the transition matrix elements for collisions that can occur. This sum is the value of the right hand side of Eq. (4) for a given  $\mathbf{n}$ , the corresponding  $w_{\mathbf{n}} = 1$  and all the other  $w_{\mathbf{m}}$  equal to zero. A single possible collision  $1 + 2 \rightarrow 3 + 4$  contributes to this sum

$$P(12 \rightarrow 34) = \frac{4\pi}{\hbar\Delta e} |U_{1234}|^2 n_1 n_2 (n_3 + 1) (n_4 + 1). \quad (13)$$

where the factor of 4 is due to different permutations of the indices which describe the same collision. We call a collision *possible* if it conserves energy and  $U_{1234} \neq 0$ , and we call  $P(12 \rightarrow 34)$  the *transition probability per unit time* for this particular collision.

### C. Ergodic approximation

In solving the QBE or the classical Boltzmann equation it is a common approximation to simplify this equation by an ergodic assumption [5,9,10,3,4]. In a classical context this corresponds to the assumption that the phase space density  $f_t(\mathbf{p}, \mathbf{x})$  only depends on the energy  $e$  of the particles at position  $\mathbf{x}$  with momentum  $\mathbf{p}$  at time  $t$ . Quantum mechanically, it is postulated that degenerate energy levels carry equal populations at all times, i.e. the populations of degenerate eigenlevels equalize on a time scale much faster than collisions between levels of different energies. This implies that the occupation numbers  $n_i$  in the QBME should be replaced by

$$n_i \rightarrow n_{\bar{i}} = \frac{1}{g_{\bar{i}}} \sum_{i \in \bar{i}} n_i, \quad (14)$$

Here we define sets of indices  $\bar{i}$  that contain all the indices of one particles states with the same energy  $\hbar\omega_{\bar{i}}$ ; and  $g_{\bar{i}}$  is the degeneracy factor of states with energy  $\omega_{\bar{i}}$ . We note that the  $n_{\bar{i}}$  are no longer integers. In our simulation this corresponds to a distribution function which is completely specified by the occupation numbers of (the block of) degenerate energy levels, i.e.  $w_{\mathbf{n}} \rightarrow w_{\bar{\mathbf{n}}}$  where  $\bar{\mathbf{n}}$  is a vector containing the number of particles in the degenerate eigenlevels  $n_{\bar{i}}$ . Removing or adding a particle to a state  $\bar{i}$  changes  $n_{\bar{i}}$  by  $1/g_{\bar{i}}$ . Therefore, we use a vector  $\mathbf{e}_{\bar{1}\bar{2}\bar{3}\bar{4}}$  which is defined by

$$\mathbf{e}_{\bar{1}\bar{2}\bar{3}\bar{4}} = [0, \dots, 0, \overset{\bar{1}}{1/g_{\bar{1}}}, 0, \dots, 0, \overset{\bar{2}}{1/g_{\bar{2}}}, 0, \dots, 0, \overset{\bar{3}}{-1/g_{\bar{3}}}, 0, \dots, 0, \overset{\bar{4}}{-1/g_{\bar{4}}}, 0, \dots, 0], \quad (15)$$

to describe collisions in the ergodic case.

Using these definitions we can write the ergodic form of Eq. (4) in the following way

$$\dot{w}_{\bar{\mathbf{n}}} = -\frac{\pi}{\hbar} \sum_{\bar{1}\bar{2}\bar{3}\bar{4}} \left( \sum_{\substack{1 \in \bar{1}, 2 \in \bar{2} \\ 3 \in \bar{3}, 4 \in \bar{4}}} \delta(\hbar(\omega_1 + \omega_2 - \omega_3 - \omega_4)) |U_{1234}|^2 \right) \times \{ n_{\bar{1}} n_{\bar{2}} (n_{\bar{3}} + 1) (n_{\bar{4}} + 1) [w_{\bar{\mathbf{n}}} - w_{\bar{\mathbf{n}} + \mathbf{e}_{\bar{1}\bar{2}\bar{3}\bar{4}}}] + (n_{\bar{1}} + 1) (n_{\bar{2}} + 1) n_{\bar{3}} n_{\bar{4}} [w_{\bar{\mathbf{n}}} - w_{\bar{\mathbf{n}} - \mathbf{e}_{\bar{1}\bar{2}\bar{3}\bar{4}}}] \}. \quad (16)$$

Transition probabilities  $P(\bar{1}\bar{2} \rightarrow \bar{3}\bar{4})$  are calculated according to

$$P(\bar{1}\bar{2} \rightarrow \bar{3}\bar{4}) = \sum_{\substack{1 \in \bar{1}, 2 \in \bar{2} \\ 3 \in \bar{3}, 4 \in \bar{4}}} P(12 \rightarrow 34) \quad (17)$$

where the sum runs over all the elements of a particular set of degenerate states. Collisions which do not change the energy distribution are thus no longer taken into account.

We note that the ergodic assumption yields the correct steady state distribution, but we expect differences in the details of the dynamics. A comparison of the kinetics with and without the ergodic assumption will be given in the case of a 3D box in Sec. III; our simulation results for the harmonic oscillator in Sec. IV will be based on the ergodic approximation.

### D. Comparison between the QBME and the QBE

Recent work of kinetics in relation to Bose condensation in trapping potentials by Holland and collaborators [5] is based on the QBE with an ergodic assumption (for a classical Boltzmann equation see also [9]). The derivation of the QBE is based on factorizing mean values  $\langle n_1 n_2 \dots n_i \rangle = \langle n_1 \rangle \langle n_2 \rangle \dots \langle n_i \rangle$  with  $\langle n_i \rangle = \sum_{\mathbf{n}} n_i w_{\mathbf{n}}$ . In the ergodic approximation one obtains

$$g_{\bar{1}} \langle \dot{n}_{\bar{1}} \rangle = \frac{4\pi}{\hbar} \sum_{\bar{2}\bar{3}\bar{4}} \{ -\langle n_{\bar{1}} \rangle \langle n_{\bar{2}} \rangle (\langle n_{\bar{3}} \rangle + 1) (\langle n_{\bar{4}} \rangle + 1) + (\langle n_{\bar{1}} \rangle + 1) (\langle n_{\bar{2}} \rangle + 1) \langle n_{\bar{3}} \rangle \langle n_{\bar{4}} \rangle \} \left( \sum_{\substack{1 \in \bar{1}, 2 \in \bar{2} \\ 3 \in \bar{3}, 4 \in \bar{4}}} |U_{1234}|^2 \delta(\hbar(\omega_1 + \omega_2 - \omega_3 - \omega_4)) \right). \quad (18)$$

In this equation  $\langle n_{\bar{i}} \rangle$  is the mean occupation of the degenerate states. The discrete  $\langle n_{\bar{i}} \rangle$  replace the particle distribution function  $f(e)$  used in the classical version [9]. The QBE describes the time evolution of the single particle distribution function in the mean distribution of the other particles. In contrast to simulations of the QBME, fluctuations in the occupation numbers are thus not described by the QBE. Moreover, it is not possible to simulate systems far from equilibrium where the factorization of the mean values is not valid. On the other hand, the QBE has the advantage that it allows simulations with much larger particle numbers than the QBME.

Since the QBME is a stochastic master equation for (quantum mechanical) occupation probabilities, we can simulate its time evolution as a series of jumps. A jump describes the collision of two particles  $1+2 \rightarrow 3+4$ , which is represented as an instantaneous change of the corresponding occupation numbers. The simulation method is often used for rate equations and works as follows:

1. Take an initial configuration of particles,  $\mathbf{n}$ , (representing an initial density operator  $\rho_\ell(t=0) = |\mathbf{n}\rangle\langle\mathbf{n}|$ ), where the energy  $E$  and the total number of particles  $N$  are fixed.
2. Calculate all the transition probabilities per unit time  $P(12 \rightarrow 34)$  for the given  $\mathbf{n}$ .
3. The *total collision rate* is now proportional to the sum over all transition probabilities per unit time.
4. The next jump occurs at time  $t_m$  since the last jump, which can be calculated by choosing a random number  $r \in ]0, 1]$  from a uniform distribution and using

$$t_m = -\frac{\ln(r)}{\sum_{1234} P(12 \rightarrow 34)}. \quad (19)$$

5. All the possible collisions are lined up with the length  $P(12 \rightarrow 34)$ . Another random number  $s \in ]0, \sum_{1234} P(12 \rightarrow 34)]$  is chosen from a uniform distribution. The transition selected by this random number  $s$  gives the particular collision  $12 \rightarrow 34$  which occurs.
6. The last step now is to set  $t := t + t_m$ ,  $|\mathbf{n}\rangle := |\mathbf{n} - \mathbf{e}_{1234}\rangle$  and  $\rho_\ell := |\mathbf{n}\rangle\langle\mathbf{n}|$ .
7. Go back to 2.
8. Repeat this simulation to obtain  $\rho = \text{constant} \times \sum_\ell \rho_\ell$ .

In every collision only four of the occupation numbers are changed and therefore only few of the transition matrix elements are modified by the change in the occupation numbers. Thus it is not necessary to calculate all transition probabilities after each step, since only those involving the  $n_1, n_2, n_3, n_4$  which define the collision will have been changed. (This is, however, more complicated than is the case for the Boltzmann master equation, where the  $1 + n_i$  factors do not occur)

For integer occupation numbers it is not possible to neglect the  $(1 + n_i)$  factors above a certain energy by arguing that the mean occupation of highly excited states is much smaller than one. For highly excited states these factors are either 1 or 2, *etc.* and cannot be replaced by 1. We have to account for them regardless of the energy of

the one-particle states involved into the collision. In our simulation method we do not restrict the number states available for the particles of the gas. We keep track of each of the particles rather than of a certain number of one-particle states. This limits the number of particles we are able to consider.

### III. 3D SQUARE WELL POTENTIAL WITH PERIODIC BOUNDARY CONDITIONS

#### A. Description of the system

First, we will simulate the QBME for a 3D cube of length  $L$  with periodic boundary conditions. This corresponds to the simplest version of the QBME. In the language of QKI  $\delta x = L$  is the length of the phase space cells. From this we immediately find the spacing of the cells in momentum to be  $\delta p = 2\pi\hbar/L$ , which is equal to the momentum spacing of the discrete energy levels in the box. The wavelet functions (introduced in QKI Eq. (26)) are therefore reduced to

$$v_{\mathbf{k}}(\mathbf{x}) = \frac{e^{i\mathbf{k}\mathbf{x}}}{L^{3/2}} \quad (20)$$

We have dropped  $\mathbf{r}$  of QKI in the equation above because there is only one phase space cell in coordinate space. The wave numbers  $\mathbf{k}$  take on the discrete values

$$\mathbf{k} = \frac{2\pi}{L}\mathbf{m} \quad (21)$$

where  $\mathbf{m}$  is a vector consisting of integer values. Since our system has the finite volume  $L^3$  the wavelet functions are orthogonal in the following sense

$$\int_{L^3} d^3x v_{\mathbf{k}_i}(\mathbf{x}) v_{\mathbf{k}_l}^*(\mathbf{x}) = \delta_{i,l} \quad (22)$$

With these wave functions we can now calculate  $U_{1234}$  to be

$$U_{1234} = \frac{4\pi\hbar^2 a}{mL^3} \delta_{\mathbf{m}_1+\mathbf{m}_2, \mathbf{m}_3+\mathbf{m}_4}. \quad (23)$$

In the case of the 3D box  $\Delta e = (2\hbar^2\pi^2)/(mL^2)$ . Using  $\sigma = 8\pi a^2$  [10] for the cross section,  $\bar{n} = N/L^3$  and  $v_1 = (2\pi\hbar)/(mL)$  which is the magnitude of velocity of a particle in the first excited state we get

$$P(12 \rightarrow 34) = \sigma \bar{n} v_1 \frac{2}{N\pi} \delta_{\mathbf{m}_1+\mathbf{m}_2, \mathbf{m}_3+\mathbf{m}_4} n_1 n_2 (n_3 + 1) (n_4 + 1). \quad (24)$$

The number of possible collisions is restricted by two Kronecker delta functions that ensure energy and momentum conservation. The overlap integral is  $U_{1234} = (4\pi\hbar^2 a)/(mL^3)$  for all the possible collisions, and does

not depend on energy or momentum of the involved one-particle states.

In semi-classical treatments of the QBE, the ergodic assumption is often made [3,4]. The density of states is approximated to be proportional to  $\sqrt{e}$ . It is then shown that the transition matrix elements are proportional to  $\sqrt{e_{\min}}$ , where  $e_{\min}$  is the minimum energy of the colliding particles (compare Appendix A). In case of a smoothly varying, strictly decreasing function  $f(e)$ , one can therefore argue that most of the collisions happen between particles with almost the same energy. In the cases we are interested in we cannot make these assumptions. The occupation numbers can vary strongly and the degeneracy of states which we count exactly is not proportional to  $\sqrt{e}$  in the energy range in which our simulations are performed.

## B. Results of simulations

All the simulations we report contain a statistical error. Unless this statistical error is given explicitly it is less than 5%.

### 1. Thermodynamic quantities

There are two ways of computing the stationary solution of the QBME (4). The first is to calculate it directly from Eq. (8); this is only feasible for very few atoms. The second possibility is to obtain the stationary solution from simulations by assuming that the time average over a sufficiently long time period equals the ensemble average. To find this time we wait until the simulation results agree with a Bose-Einstein distribution Eq. (9). This also allows us to assign a temperature  $T$  to the system. All the results are scaled to the critical temperature in the thermodynamic limit  $T_c = 2\hbar^2\pi/(mL^2k)(N/\zeta(3/2))^{2/3}$  [11]. There are three parameters of the system;  $E$ ,  $L$  and  $N$  which give a certain  $T$ ,  $T_c$  and  $N$  in thermodynamic equilibrium. In the simulation we fix  $E$  and  $N$ , and the scaling to the critical temperature is equivalent to scaling to a certain particle density  $N/L^3$  in the box.

The expression  $T_c$  for the critical temperature is, of course, only valid in the thermodynamic limit because in the derivation [12] sums over energies are replaced by integrals which over- or underestimate the sums for finite systems depending on the density of states. In the thermodynamic limit the energy spectrum becomes continuous and summing yields the same result as integrating. For a finite number of particles we therefore do not expect the critical temperature and the condensate fraction vs. temperature to be the same as in thermodynamic limit.

Fig. 1 shows the comparison of the results from the simulations and the grand canonical expression Eq. (10).

The degeneracies  $g_i$  in Eq. (10) are calculated by counting all ways of combining different integer numbers  $m_i^x, m_i^y, m_i^z$  consistent with the definite energy

$$\hbar\omega_i = \frac{2\pi^2\hbar^2}{mL^2} \left( (m_i^x)^2 + (m_i^y)^2 + (m_i^z)^2 \right). \quad (25)$$

The simulation and the grand canonical result both give a higher number of particles in the condensate than expected from the thermodynamic result. The results for finite number of particles, however, approach the thermodynamic limit with increasing  $N$  very quickly. Around the critical temperature there is a slight deviation of the simulated results from the grand canonical results [13], whereas for  $T \ll T_c$  there is almost no difference. This is due to a bigger statistical error in the simulation because of the large fluctuations in the region around the critical temperature. Note also that we are comparing two different statistical ensembles, and that for finite systems we would not expect exact agreement between the results from different ensembles.

### 2. Occupation of the ground state

We want to investigate the scaling of the one-particle state occupation with the number of particles in the gas. For BEC we expect [8] the occupation of the ground state to be

$$\frac{n_0}{L^3} = \frac{N}{L^3} \left( 1 - \left( \frac{T}{T_c} \right)^{3/2} \right), \quad (26)$$

while for excited states

$$\frac{\langle n_i \rangle}{L^3} \leq \frac{T}{L} \times \frac{mk}{2\pi^2\hbar^2\mathbf{m}_i^2} \xrightarrow{L \rightarrow \infty} 0. \quad (27)$$

Fig. 2 shows the occupation numbers of the ground state and the first excited state. At a given  $T/T_c$  the number of particles in the ground state increases linearly with the total number, whereas the slope of the occupation of the first excited state becomes smaller with increasing number of particles. From this numerical result we conclude that the QBME does really describe a macroscopic occupation and is consistent with expecting BEC below the critical temperature  $T_c$ .

### 3. Collision times with and without the ergodic assumption

Obviously, the results given in previous Secs. IIIB 1 and IIIB 2 are the same with or without use of the ergodic assumption. This is expected, because in thermal equilibrium all degenerate eigenlevels should have the same occupation number even without the ergodic assumption. The mean time between two collisions in thermal equilibrium is computed by taking the average over all the

calculated times  $t_m$  from Eq. (19). This time has to be multiplied by  $N/2$  because one particular particle is involved in one out of  $N/2$  collisions.

In Fig. 3 we plot the mean collision time  $t_{\text{coll}}^{\text{ne}}$  for one particle versus the temperature without the ergodic assumption. The classical elastic mean collision time calculated from  $t_{\text{coll}}^c = (\sigma \bar{n} v_T)^{-1}$ , where  $v_T$  is the mean thermal velocity of the gas  $v_T = N^{-1} \sum_i \sqrt{(2\hbar\omega_i)/(m)} \langle n_i \rangle$ , and  $\langle n_i \rangle$  is the mean occupation of the  $i$ -th energy level obtained from the simulation. As soon as the gas becomes degenerate the  $1 + n_i$  factors in Eq. (4) become important and increase the collision rate compared to the classical case. For temperatures close to zero the collision time increases again because there are only few particles outside the condensate which can take part in collisions. Fig. 4 shows the comparison between the curves for the ergodic collision time  $t_{\text{coll}}^c$  and  $t_{\text{coll}}^{\text{ne}}$ . For very small temperatures, the ergodic assumption allows for collisions which can not occur in the non-ergodic case because the corresponding states are not occupied. As soon as the temperature is close to  $T_c$ , those collisions in the non-ergodic case that only change the direction of the momentum of an individual particle decrease  $t_{\text{coll}}^{\text{ne}}$  compared to the ergodic case. Since this type of collisions leaves the energy of the particles unchanged they are not included in the ergodic calculations.

#### 4. Particle distributions

While the mean values for the occupation numbers are easy to calculate it takes more effort to find the particle distribution  $W_i(j)$  of the one-particle states. There are two ways of calculating these distributions. Either we calculate the time a state was occupied by a certain number of particles (time average) or we record the number of particles in that state after a certain time for many different trajectories (ensemble average). Both results need not necessarily be the same unless the system has the stationary solution Eq. (8). We used both methods to calculate particle distributions for the condensate and some of the excited states for different temperatures.

In Fig. 5 particle distributions for the ground state are plotted. Particle distributions of the condensate are well approximated by a Gaussian for temperatures below  $T_c$ . However, they are not completely symmetric around the mean value like the Gaussian there is a slight asymmetry which increases with temperature. The shape of the distribution changes close to the critical temperature. For  $N = 500$  at  $T = 1.1T_c$  the distribution develops a second local maximum at  $N_c = 0$  and at  $T = 1.2T_c$  the peak at finite number of condensate particles has disappeared. Well above  $T_c$  at  $T = 1.7T_c$  it agrees with a Bose-Einstein distribution

$$p(N_c) = (1 - \eta)\eta^{N_c} \quad (28)$$

with  $\langle N_c \rangle = \eta/(1 - \eta)$ .

The particle distribution of the first excited state in Fig. 6 can be approximated by the Bose-Einstein distribution (28) for  $T \ll T_c$  and  $T \gg T_c$ . Particle distributions of highly excited states agree with the Bose-Einstein probability distribution (28) at all temperatures.

In Fig. 7 we plot the standard deviation  $\sigma(N_c)$  of the particle distribution of the condensate in thermal equilibrium. The error bars are calculated according to  $\sqrt{\sigma((N_c - \langle N_c \rangle)^2)/\langle N_c \rangle}$  which is the variance of the standard deviation normalized to the mean number of particles in the condensate. This gives the mean deviation of the standard deviation from its calculated value. For small temperatures  $\sigma(N_c)$  rises almost linearly with temperature. The number of possible states with different number of particles in the condensate increases which leads to a larger width of the distribution. Close to  $T_c$  we get a very broad particle distribution with a very large standard deviation. For  $T > T_c$  the standard deviation will tend to go to the mean number of particles in the condensate which agrees with the fit to the Bose-Einstein distribution which has a standard deviation of  $N_c(N_c + 1)$  going to  $N_c$  for  $N_c \ll 1$ .

This also agrees with the calculation performed in Sec. IIB2 for the case of very small mean occupation of a state. At small temperatures we calculate the particle distribution in the condensate according to Eq. (12). To compute the sum in Eq. (12) we assume that most of the fluctuations come from exchange of particles of the condensate with the first few excited states. The particles in higher excited states should not have a significant influence on the fluctuations in the condensate, but they should ensure that particles in the lowest lying states can be distributed among degenerate eigenlevels, without restrictions due to conservation laws. The derivation of Eq. (12) is based on the assumption that the particle distribution among degenerate eigenlevels is not restricted by conservation laws. Using Eq. (12) we obtain particle number fluctuations of the condensate due to exchange with low lying levels. In particular we calculate  $W_0(j)$  from Eq. (12) by taking into account the first seventeen energy levels. The particle distributions we get agree well with the ones from the simulations. In Fig. 7 the results of both calculation methods are compared for temperatures  $T < 0.5T_c$ . The crosses correspond to the numerical calculations on Eq. (12) and agree well with the simulation results.

#### 5. Growth of the condensate

Here we want to investigate how the condensate builds up when the simulation is started in a non-equilibrium distribution. As the initial state we choose a Gaussian-like distribution: We first distribute the particles randomly into states with energies between that of the first excited state, and twice the mean energy, and then move particles to higher or lower energy states until the given

fixed energy  $E$  of the system is exactly reached.

Whenever possible we avoid putting particles in the condensate at the beginning of the simulation. As can be seen in Fig. 8 the condensate growth is well fitted by  $N_c(1 - \exp(-t/\tau))$  where  $N_c$  is the number of particles in the condensate in thermal equilibrium and the time constant  $\tau$  is found by fitting this function to the simulation. This holds as long as the fraction of condensate particles in thermal equilibrium is not much less than one.

#### 6. Time to reach an ergodic distribution

While with the ergodic assumption all degenerate levels are equally occupied at all times, in the non-ergodic case collisions themselves are responsible for equalizing the occupations of degenerate levels. To check the relaxation time for a distribution to become ergodic we disturb a system in thermal equilibrium by putting *all* particles with energy  $\Delta e$  into *two* of the first excited states (with opposite momentum so that the total momentum is unchanged). As is shown in Fig. 9 the particle distribution comes to equilibrium in approximately  $10 t_{\text{coll}}^{\text{ne}}$ . Collisions, therefore, transfer the occupation between degenerate levels at a time scale of the order of the mean collision time in the gas. We conclude that for the ergodic assumption to be valid strictly speaking it is only reasonable to look at quantities that are mean values over several collision times.

## IV. 3D ISOTROPIC HARMONIC OSCILLATOR

### A. Description of the system

In this section we will study Bose particles trapped in an isotropic harmonic trap with trap frequency  $\omega$ . The vector  $|\mathbf{n}\rangle$  now gives the occupations of the trap levels, and  $U_{1234}$  contains the spatial eigenfunctions of the harmonic oscillator. For the low lying levels these integrals can be evaluated numerically but for highly excited states it is difficult to get reliable results for  $U_{1234}$ . Therefore, we will limit ourselves to using the ergodic form of the QBME as explained in Sec. II C. As is shown in [10], the transition matrix elements of transitions which change the energy distribution function can be approximated by

$$\begin{aligned} P(\bar{1}\bar{2} \rightarrow \bar{3}\bar{4}) &= \frac{4\pi}{\hbar^2\omega} \frac{m\sigma\omega^3\hbar}{4\pi^3} g_{\min(\bar{1}\bar{2}\bar{3}\bar{4})}^h \\ & n_{\bar{1}}n_{\bar{2}}(n_{\bar{3}}+1)(n_{\bar{4}}+1) \\ &= \bar{n}_h^0\sigma v_0(2N)^{-1} g_{\min(\bar{1}\bar{2}\bar{3}\bar{4})}^h \\ & n_{\bar{1}}n_{\bar{2}}(n_{\bar{3}}+1)(n_{\bar{4}}+1) \end{aligned} \quad (29)$$

Here  $g_j^h = (j+1)(j+2)/2$  is the degeneracy factor of the  $j$ -th eigenstate with energy  $j\hbar\omega$ ,  $v_0 = \sqrt{(4\hbar\omega)/(\pi m)}$

the mean magnitude of velocity of a particle in the ground state of the oscillator, and  $\bar{n}_h^0$  is the mean particle density if all the particles are within a cube of length  $\sqrt{(\hbar\pi)/(m\omega)}$ . This is the semi-classical expression obtained in Appendix A. According to Ref. [10] numerical calculation shows that this expression is a good approximation even for low lying energy levels.

## B. Results of simulations

### 1. Stationary solutions

To obtain the grand canonical stationary solutions for the 3D harmonic oscillator we have to replace  $g_i$  by  $g_i^h$  in the Eq. (10). The critical temperature for an ideal Bose gas in a 3D isotropic trap in the thermodynamic limit (i.e. when the sums over the discrete energy levels are replaced by integrals) is given by  $T_c = (\hbar\omega)/k(N/\zeta(3))^{1/3}$  [12]. Our simulation results for the condensate fraction versus temperature are shown in Fig. 10. The continuum approximation increases the condensate fraction for finite number of particles compared to the simulation results. The reason for this is that the density of states rises much faster than for the 3D box. As in the case of the square well potential, the results for the microcanonical simulations and the grand canonical calculations agree very well. Comparing the two curves for  $N = 500$  of Fig. 1 and Fig. 10 we find that the phase transition is more pronounced in the harmonic oscillator compared to the much smoother transition for the 3D box. This behavior can also be seen by plotting of the energy versus temperature in Fig. 11. There is a visible change in the slope of the energy for the harmonic oscillator even for  $N = 500$ . For the ideal gas the heat capacity has a jump at the critical temperature in the thermodynamic limit in the harmonic oscillator whereas in case of the 3D box only the slope of the heat capacity is discontinuous at the critical temperature [12]. This makes clear that the thermodynamically expected differences in the condensation process between the harmonic oscillator and the free gas can also be seen in finite systems for small particle numbers.

### 2. Collision times

We will now compare the mean collision time obtained in our simulations  $t_{\text{coll}}^{\text{he}}$  with the elastic collision time defined as  $t_{\text{coll}}^{\text{hc}} = (\bar{n}_h\sigma v_{\text{Th}})^{-1}$ . We determine  $v_{\text{Th}}$  and  $\bar{n}_h$  with the assumption that the kinetic energy of the particles are equal potential energy equally. Then we find for the mean density and the thermal velocity  $\bar{n}_h = (3N)/(4\pi)((m\omega^2)/(E_{3/2}))^{3/2}$  and  $v_{\text{Th}} = \sqrt{E_{1/2}/m}$  respectively, with  $E_s = (1/N \sum_i (\hbar\omega_i)^s \langle n_i \rangle)^{1/s}$ .

In Fig. 12 we plot the mean collision time versus temperature. For temperatures higher than the critical tem-

perature the simulation agrees well with the classical result (dashed curve). For temperatures far below  $T_c$ , the result of the simulation is approximately equal to the dotted curve which we obtained by the assumption that the size of the cloud is the ground state size and only the thermal velocity varies with temperature. Around the critical temperature the size of the cloud shrinks faster than expected from the classical approximation.

### 3. Evaporative cooling

Currently BEC is achieved in experiments by evaporative cooling, i.e. by removing particles with a high energy from the trap (for a review see [14]). Elastic collisions between the particles thermalize the particle distribution which leads to a decreasing temperature. To simulate a Bose gas that is evaporatively cooled we cut off the trap at a certain energy level  $E_b(t)$ , with  $E_b(t)$  a given function of time. Each particle which is scattered into an energy level above  $E_b(t)$  after a collision is considered as lost. In our simulations we start with  $N_0 = 800$  particles in the thermodynamic equilibrium at a temperature of  $T \approx 1.4T_c$ . Then all particles with an energy larger than  $E_b(t = 0) = 65\hbar\omega$  are removed. During the simulation we decrease  $E_b$  exponentially according to

$$E_b(t) = (E_b(0) - E_l)e^{-\gamma t} + E_l, \quad (30)$$

where  $E_l = 8\hbar\omega$ . In Fig. 13 the total number of particles in the gas  $N$  and the number of particles in the condensate  $N_c$  are plotted as a function of time for different parameters  $\gamma$ . First the particles in the highest energy levels are evaporated quickly. During the cooling process, the collision time decreases by an order of magnitude as shown in Fig. 14; nevertheless the number of particles evaporated per unit time does not increase during the cooling process. The reason is that most of the collisions occur between particles with almost the same energy and thus many collisions are necessary to redistribute the particles when some of them are evaporated. If the collision rate did not increase so rapidly particles might be lost from the trap faster than evaporative cooling is possible. As soon as the condensate builds up the mean collision time increases again. This expected behavior agrees qualitatively with Fig. 12.

In order for the evaporative cooling to be efficient it is important to quickly put as many particles as possible into the condensate. We therefore have calculated the size of the condensate divided by the time needed to reach 90% of the equilibrium condensate fraction for different values of  $\gamma$  as shown in Fig. 15. The size of the condensate is limited by the initial number of particles in the gas, the initial size of the cut-off  $E_b(0)$ , and the initial energy  $E$  (for  $\gamma \ll t_{\text{coll}}^{-1}$ ). For  $\gamma \geq t_{\text{coll}}^{-1}$  only few collisions will occur while the cut-off is ramped down. The number of particles that reach the condensate is therefore mainly determined by the collision rate. As can be seen from

the Fig. 15 there is a value for the ramp rate  $\gamma$  which maximizes the number of particles transferred into the condensate per unit time, and therefore optimizes the cooling process under the assumption that additional loss rates from the trap do not change while the gas is cooled.

We also performed some evaporative cooling simulations for a gas in a 3D-box. Because the density of states in that case does not rise as quickly as in the harmonic oscillator particle energies are changed more during a collision than in the harmonic oscillator. Therefore it is also possible to evaporatively cool a gas in a box quickly although the collision rate does not rise as much as in the harmonic trap.

## V. CONCLUSIONS

We have simulated stationary and non-stationary properties of a Bose gas in a trapping potential with finite number of particles in the framework of the Quantum Boltzmann Master Equation.

For a gas confined in a 3D-box we have found that the number of particles in the condensate at a given temperature is larger than expected from the thermodynamic limit. We have also computed the mean collision time of particles in the gas. Comparison with the classical result shows that boson statistics tends to decrease the collision time close to the critical temperature. Calculations of fluctuations in the number of particles in the one-particle ground state have shown that the standard deviation increases almost linearly with temperature until the critical temperature is reached. For temperatures above  $T_c$  the standard deviation decreases again, and the distribution becomes Poissonian for high temperatures. We have also found that population is transferred at a time scale of the order of the collision time which is important for the range of validity of the ergodic form of the QBME.

Our simulations of a Bose gas in an isotropic harmonic trap were restricted to the ergodic form of the QBME. In contrast to the 3D box the number of particles in the condensate is decreased relative to the usual continuum (thermodynamic) limit at a given temperature. We found that the mean collision time decreases significantly as temperature reaches the critical point from above. This is due to the increase of the density, as soon as the ground state is macroscopically occupied. Simulations of evaporative cooling have shown that there is an ramp rate to lower the cut-off energy of the trap with the goal of transferring as many particles as possible per unit time to the ground state.

The present formalism is readily extended to include mean field effects, and pumping and loss of particles from a degenerate Bose gas. This is relevant for modeling atom lasers based on collisions [15,16].

Acknowledgment: D.J. thanks JILA for hospitality, supported by a fellowship from the University of Inns-

bruck, and for very stimulating and useful discussions with M. Holland, and J. Cooper. D.J. and P.Z. were supported in part by the Austrian Science Foundation. C.W.G. is supported by The Marsden Fund. Part of this work was supported by TMR network ERB 4061 PL 95-0044.

## APPENDIX A: THE CLASSICAL LIMIT

To connect the present paper with Ref. [9] we briefly rederive the classical Boltzmann equation with the ergodic approximation from the QBE (18). We assume the distance between energy levels small compared to the mean energy of a particle so that the sum can be replaced by an integral. In the classical limit we get for the density of states at energy  $e$

$$\rho(e) = \frac{1}{(2\pi\hbar)^3} \int d^3p d^3x \delta\left(e - U(\mathbf{x}) - \frac{\mathbf{p}^2}{2m}\right), \quad (\text{A1})$$

where  $U(\mathbf{x})$  is the trapping potential. The degeneracy of the coarse grained one-particle states  $g(e)$  is connected to the density of states by  $g(e) = \Delta e \rho(e)$ . We replace

$$\sum_{i \in \bar{i}} \Psi_i^*(\mathbf{x}) \Psi_i(\mathbf{x}') \rightarrow \frac{\Delta e}{(2\pi\hbar)^3} \int d^3p_i \delta\left(e_i - U(\mathbf{x}) - \frac{\mathbf{p}_i^2}{2m}\right) e^{i(\mathbf{x}-\mathbf{x}') \cdot \mathbf{p}_i / \hbar}, \quad (\text{A2})$$

where  $e_i = \hbar\omega_i$ . The factor  $\Delta e$  in Eq. (A2) ensures the normalization of the sum over the wavefunctions to  $g(e_i)$ . Inserting replacement Eq. (A2) into  $|U_{1234}|^2$  and integrating over  $\mathbf{x}'$  yields a  $\delta$ -function of the four momenta times  $(2\pi\hbar)^3$ . Integrating over  $\mathbf{p}_4$  i.e. setting  $\mathbf{p}_4 = \mathbf{p}_1 + \mathbf{p}_2 - \mathbf{p}_3$  we obtain

$$\sum_{\substack{1 \in \bar{1}, 2 \in \bar{2} \\ 3 \in \bar{3}, 4 \in \bar{4}}} |U_{1234}|^2 \delta(e_1 + e_2 - e_3 - e_4) = \frac{16\pi^2 \hbar^4 a^2}{m^2} \frac{\Delta e^4}{(2\pi\hbar)^9} \int d^3p_1 d^3p_2 d^3p_3 \prod_{i=1}^4 \delta\left(e_i - U(\mathbf{x}) - \frac{\mathbf{p}_i^2}{2m}\right) \delta(e_1 + e_2 - e_3 - e_4). \quad (\text{A3})$$

We define the total momentum  $\mathbf{P} = \mathbf{p}_1 + \mathbf{p}_2$  and the relative momenta  $\mathbf{q}' = (\mathbf{p}_1 - \mathbf{p}_2)/2$  and  $\mathbf{q} = (\mathbf{p}_3 - \mathbf{p}_4)/2$ . Integrating over the azimuthal angles of the two relative momenta  $\mathbf{q}$  and  $\mathbf{q}'$  and over the length of the relative momentum  $\mathbf{q}$  and calculating the remaining integral similarly to [9] we obtain

$$\sum_{\substack{1 \in \bar{1}, 2 \in \bar{2} \\ 3 \in \bar{3}, 4 \in \bar{4}}} |U_{1234}|^2 \delta(e_1 + e_2 - e_3 - e_4) = \frac{2m\Delta e^4 a^2}{\pi^2 \hbar^2} \rho(e_{\min}) \delta(e_1 + e_2 - e_3 - e_4). \quad (\text{A4})$$

We insert expression (A4) into the QBE (18), divide by  $\Delta e$ , replace the notation  $\langle n_i \rangle$  by  $f(e_i)$  and the  $\sum \Delta e^3$  by  $\int de_2 de_3 de_4$  and obtain finally

$$\rho(e_1) f(e_1) = \frac{8\pi m a^2}{\pi^2 \hbar^3} \int de_2 de_3 de_4 \delta(e_1 + e_2 - e_3 - e_4) \{-f(e_1) f(e_2) + f(e_3) f(e_4)\} \rho(e_{\min}). \quad (\text{A5})$$

In Eq. (A5) the  $(1+f)$  factors are neglected by assuming that in the classical limit the mean occupation of a quantum level is much less than one. Setting  $\sigma = 8\pi a^2$  this is the ergodic form of the classical Boltzmann equation from Ref. [9].

- 
- [1] C.W. Gardiner and P. Zoller (to appear in Phys. Rev. A).
  - [2] C.W. Gardiner and P. Zoller (unpublished).
  - [3] Yu. M. Kagan, B.V. Svistunov and G.V. Shlyapnikov, JETP **75**, 387 (1992).
  - [4] D.V. Semikoz and I.I. Tkachev, Phys. Rev. Lett. **74**, 3093 (1995).
  - [5] M. Holland, J. Williams, K. Coakley, and J. Cooper, Quantum Semiclass. Opt. **8**, 571 (1996).
  - [6] The description of the system can be extended from a binary collision model to a T-matrix description of the interaction between the particles.
  - [7] Note that we concentrate a whole energy region into the one-particle ground state of the system. Therefore, onset of BEC means to get a macroscopic occupation in this energy region not in a single quantum state.
  - [8] K. Huang, *Statistical Mechanics* (John Wiley & Sons, New York, 1987).
  - [9] O.J. Luiten, M.W. Reynolds and J.T.M. Walraven, Phys. Rev. A **53**, 381 (1996).
  - [10] M. Holland, J. Williams, and J. Cooper (unpublished).
  - [11] R.K. Pathria, *Statistical Mechanics* (Pergamon, New York, 1972), Vol. 45.
  - [12] V. Bagnato, D.E. Pritchard, and D. Kleppner, Phys. Rev. A **35**, 4354 (1987).
  - [13] S. Grossmann and M. Holthaus, Phys. Rev. E. **54**, 3495 (1996).
  - [14] W. Ketterle and N.J. van Druten (unpublished).
  - [15] M. Holland, K. Burnett, C. Gardiner, J.I. Cirac, and P. Zoller, Phys. Rev. A **54**, R1757 (1996).
  - [16] H.M. Wiseman (unpublished).

FIG. 1. Condensate fraction versus temperature in thermal equilibrium for the 3D square well potential. (a) thermodynamic limit, (b) grand canonical solution for  $N = 500$  (solid line) and results from the simulation (+), (c) grand canonical solution for  $N = 100$  (solid line) and results from the simulation (o).

FIG. 2. Occupation numbers for the ground state  $N_c$  and the first excited state  $n_1$  against the total number of particles  $N$  in thermal equilibrium for  $T = 0.5 T_c$ .

FIG. 3. Mean collision time per particle versus temperature for  $N = 500$  of the 3D box without ergodic assumption. Result of the simulation (+) and result for  $t_{\text{coll}} = (\sigma \bar{n} v_T)^{-1}$  (dashed line). The time scale is normalized to  $(\bar{n} \sigma v_1 2/N)^{-1}$ .  $v_1$  is the magnitude of velocity of a particle in a first excited state as defined in the text.

FIG. 4. Mean collision time per particle versus temperature for  $N = 100$  for the 3D box. Result of the simulation without (b) and with (a) the ergodic assumption, result for  $t_{\text{coll}} = (\sigma \bar{n} v_T)^{-1}$  (dashed line). The time scale is normalized to  $(\bar{n} \sigma v_1 2/N)^{-1}$ .  $v_1$  is the magnitude of velocity of a particle in a first excited state as defined in the text.

FIG. 5. Probability distribution of particles in the condensate for the 3D harmonic box without the ergodic assumption. Results of the simulation (bars) and fits (solid lines) are calculated for  $N = 500$ .

FIG. 6. Probability distribution of particles in one of the first excited states for the 3D box without the ergodic assumption. Results of the simulation (bars) and fits (solid lines) are calculated for  $N = 500$ .

FIG. 7. Fluctuation of the condensate fraction versus temperature in thermal equilibrium for the 3D square well potential. Results of the simulation for  $N = 500$ . The crosses give the results from the numerical summation of Eq. (12). The dashed line is  $\sqrt{N_c}$  which would be equal to  $\sigma(N_c)$  if the fluctuations in the condensate were Poissonian.

FIG. 8. Buildup of the condensate for the 3D box for  $N = 500$ . The energy is chosen such that in equilibrium  $T = 0.5 T_c$ . The time scale is normalized to  $(\bar{n} \sigma v_1 2/N)^{-1}$  in thermal equilibrium. The dashed line is a fit of the form  $N_c(1 - \exp(-t/\tau))$ , with  $\tau = 0.0013$  and  $N_c = 368$ , as explained in the text.

FIG. 9. Distortion of an ergodic distribution into a non ergodic one for the 3D box. Particle distribution of the depleted levels ( $P(n_1^i)$ ) and of the filled levels ( $P(n_1^f)$ ) at time  $t$  after the distortion. Simulation for  $N = 500$  at  $T = 0.4 T_c$ .

FIG. 10. Condensate fraction versus temperature in thermal equilibrium for the 3D harmonic oscillator. (a) thermodynamic limit, (b) grand canonical solution for  $N = 500$  (solid line) and results from the simulation (+), (c) grand canonical solution for  $N = 300$  (solid line) and results from the simulation (o).

FIG. 11. Total energy of the system versus temperature. (a) data for harmonic oscillator, (b) data for the 3D box each with  $N = 500$ . Energy is normalized to the level spacing  $\Delta e$ . (+) results from the microcanonical simulation; (solid line) result of the grand canonical calculation.

FIG. 12. Mean collision time per particle versus temperature for  $N = 500$  for the harmonic oscillator. Result of the simulation (solid line) and result for  $t_{\text{coll}} = (\sigma \bar{n}^h v_T)^{-1}$  (dashed line). The dotted line shows the collision time with the assumption of a fixed density equal to the ground state density. The time scale is normalized to  $(\bar{n}_h^0 \sigma v_0 2/N)^{-1}$ .  $v_0$  is the amount of velocity of a particle in the ground state as defined in the text.

FIG. 13. Total number of particles  $N$  and number of particles in the condensate  $N_c$  for  $\gamma = 1/10$  (solid line)  $\gamma = 1/2$  (dashed line) and  $\gamma = 3/2$  (dotted line) against time  $t$ .  $\gamma$  is the time constant from Eq. (30) normalized to  $\sigma \bar{n}_h^0 v_0 2/N$ . The time  $t$  is normalized to  $(\sigma \bar{n}_h^0 v_0 2/N)^{-1}$ .

FIG. 14. Mean collision time  $t_{\text{coll}}$  versus time  $t$  for  $\gamma = 1/10$  (solid line)  $\gamma = 1/2$  (dashed line) and  $\gamma = 3/2$  (dotted line) against time  $t$ .  $\gamma$  is the time constant from Eq. (30) normalized to  $\sigma \bar{n}_h^0 v_0 2/N$ . The time  $t$  is normalized to  $(\sigma \bar{n}_h^0 v_0 2/N)^{-1}$ .

FIG. 15. Size of condensate divided by time to reach 90% of the final size of the condensate versus time constant  $\gamma$ .  $\gamma$  is the time constant from Eq. (30) normalized to  $\sigma \bar{n}_h^0 v_0 2/N$ .

Fig. 1

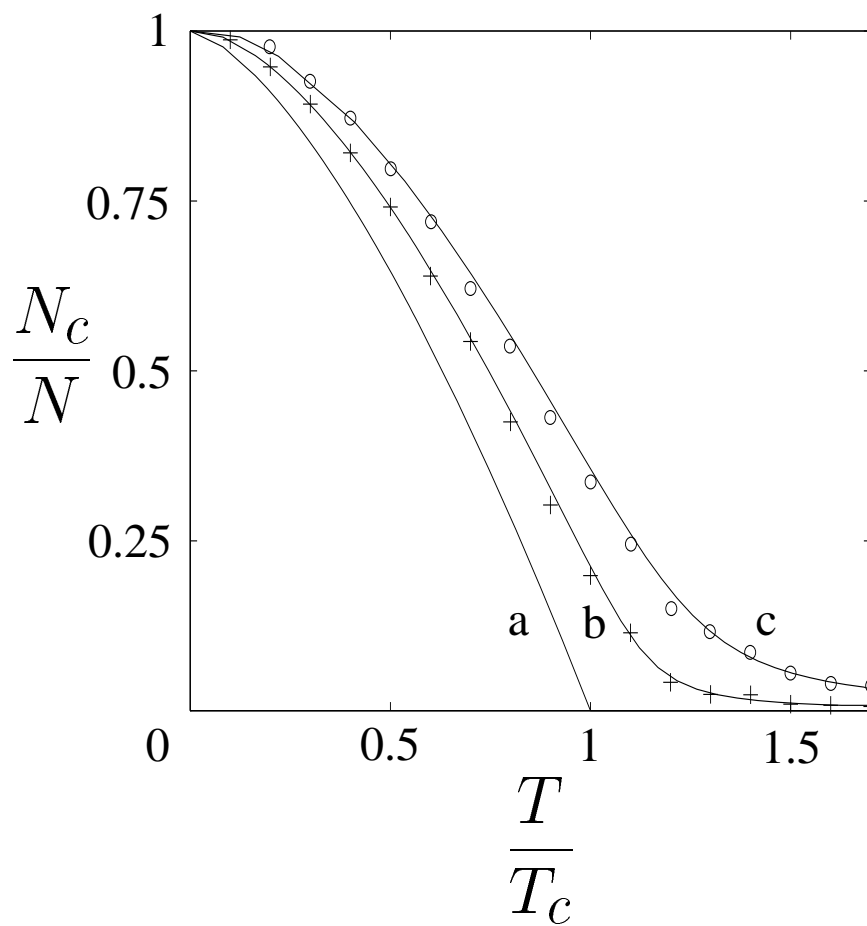


Fig. 2

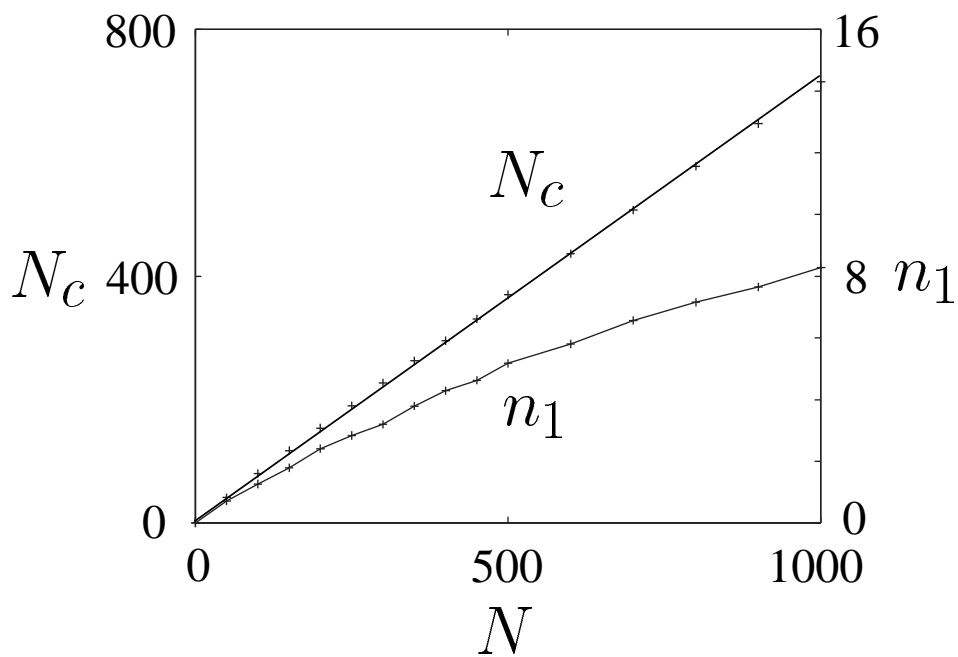


Fig. 3

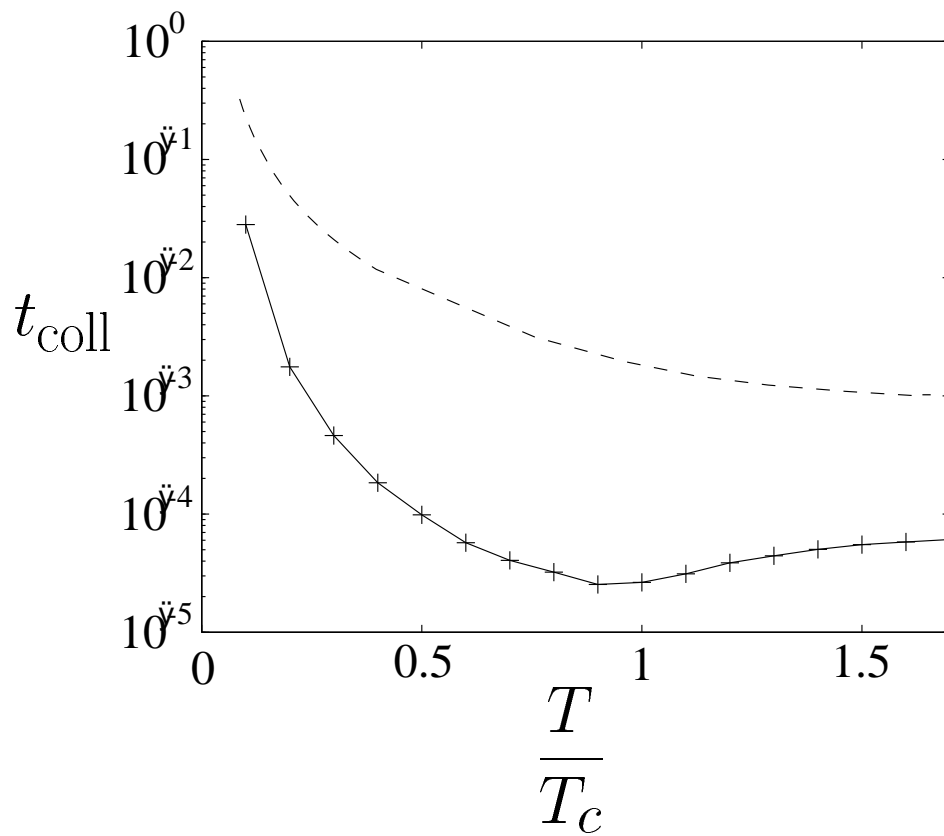


Fig. 4

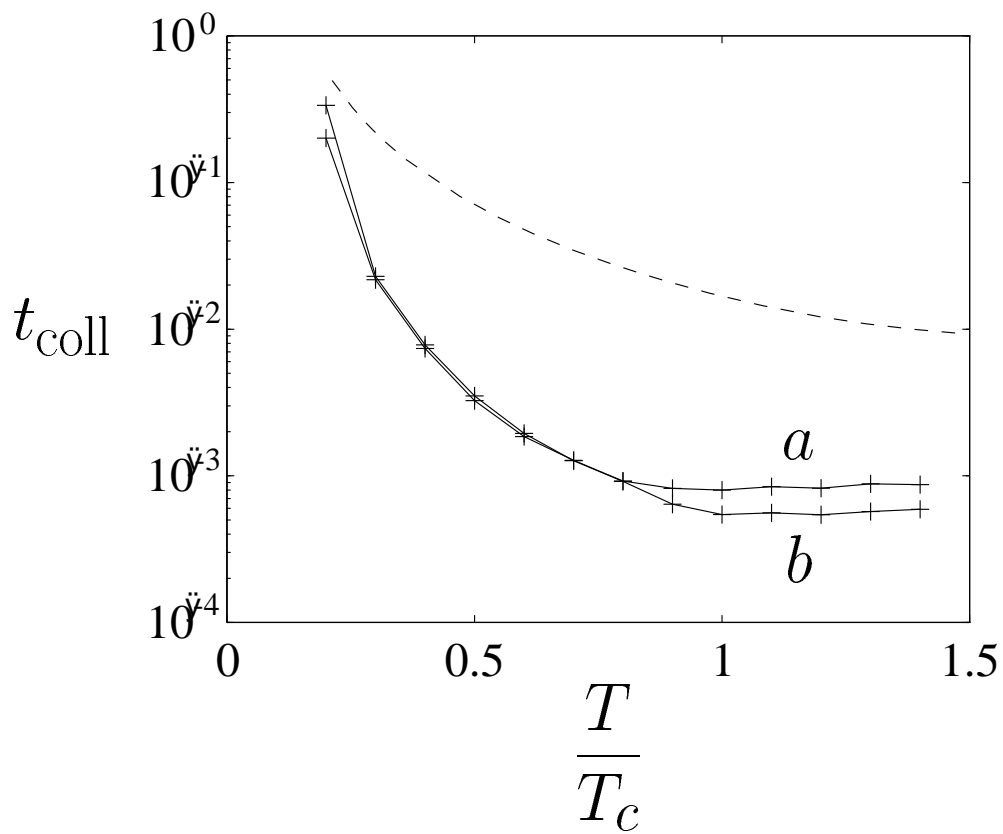


Fig. 5

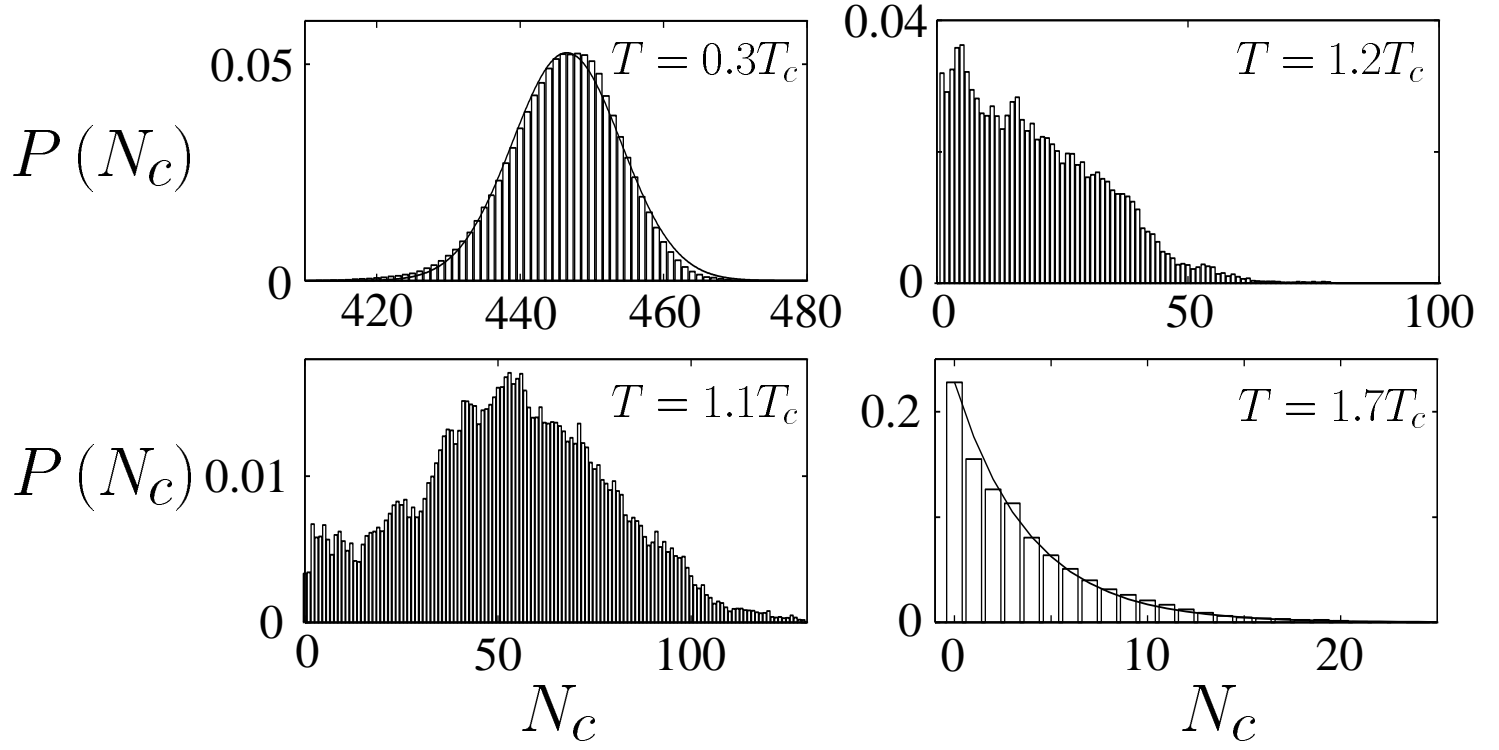


Fig. 6

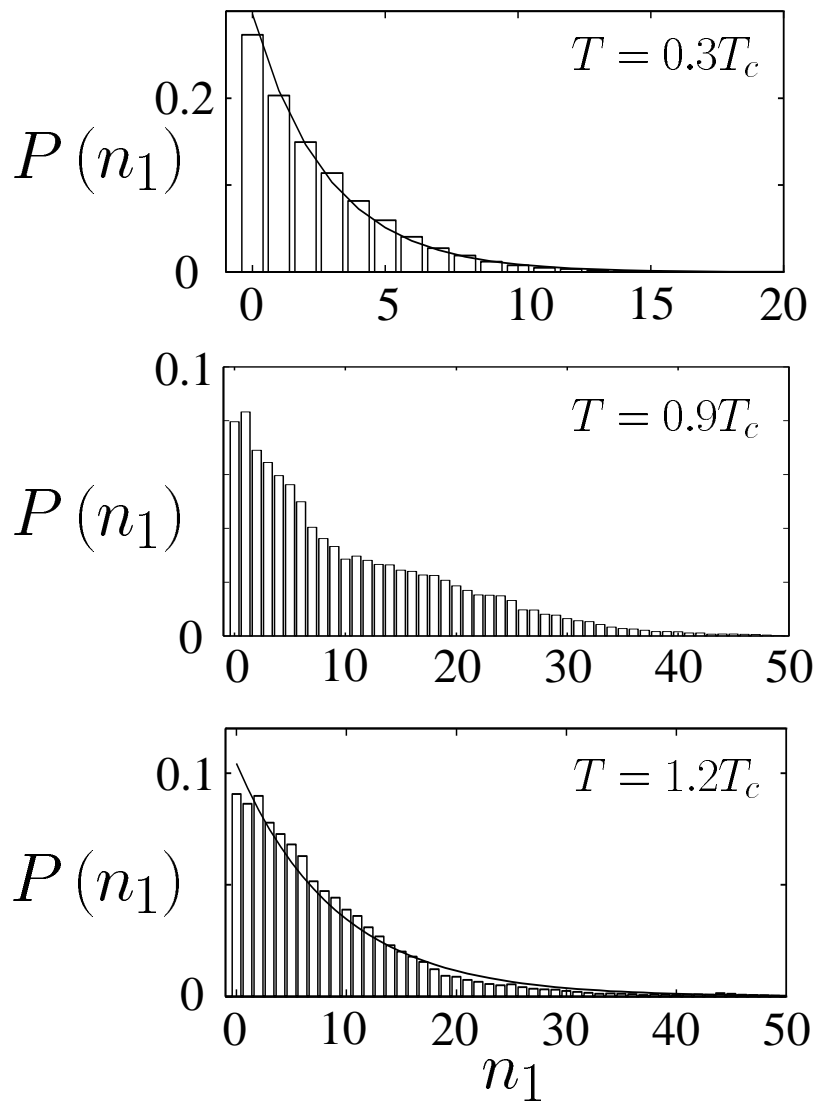


Fig. 7

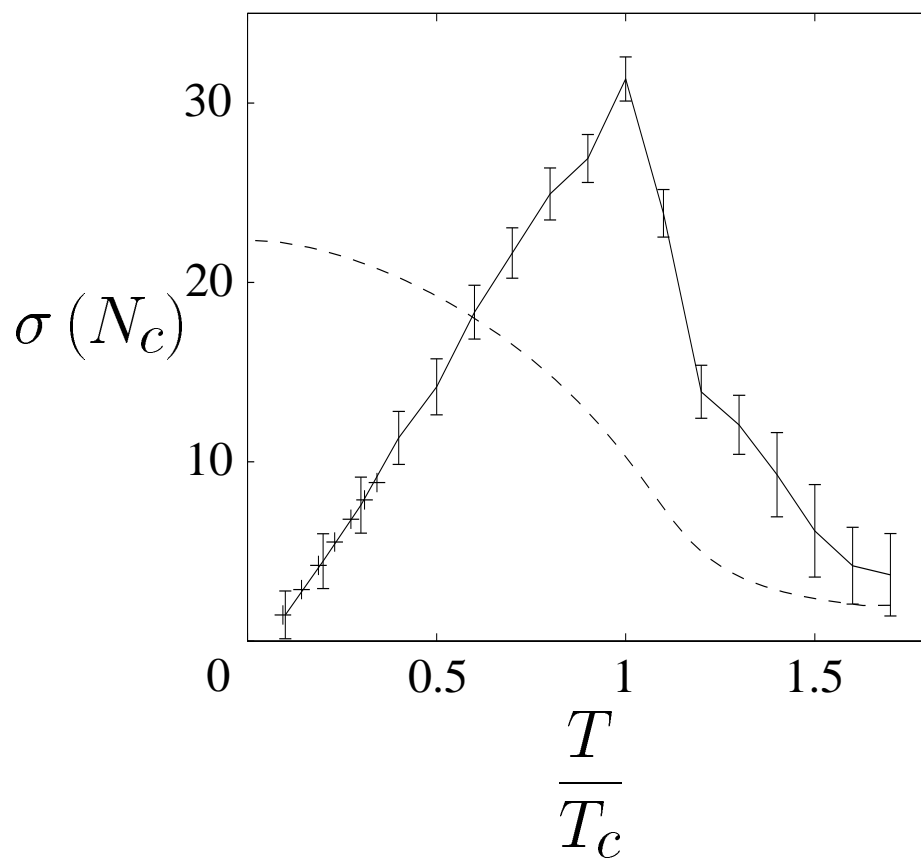


Fig. 8

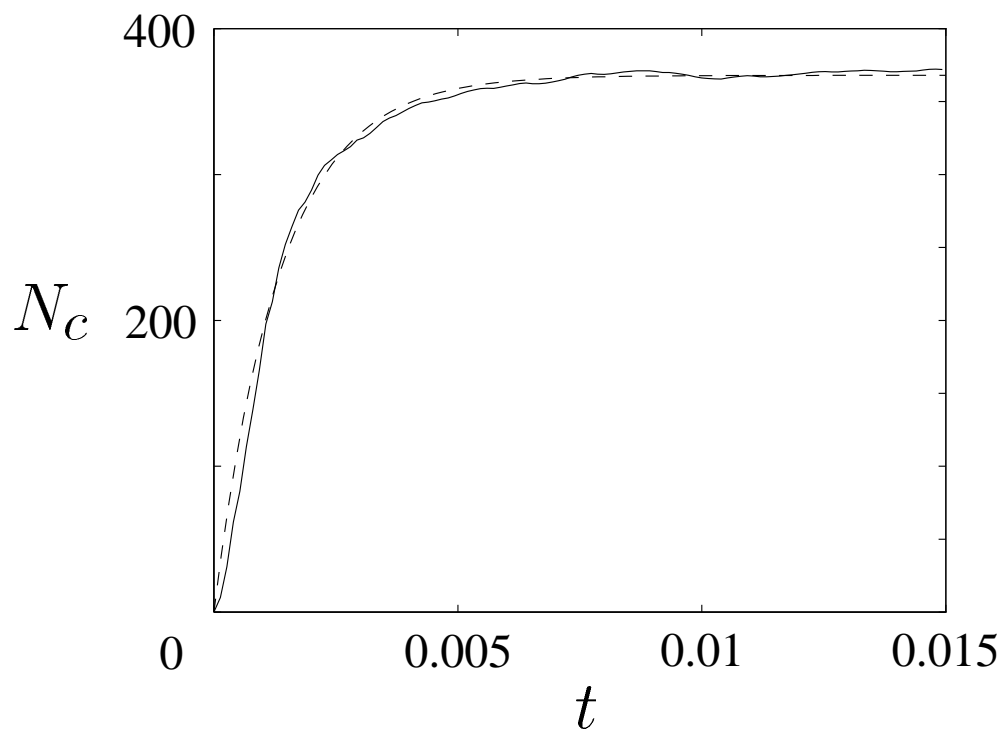


Fig. 9

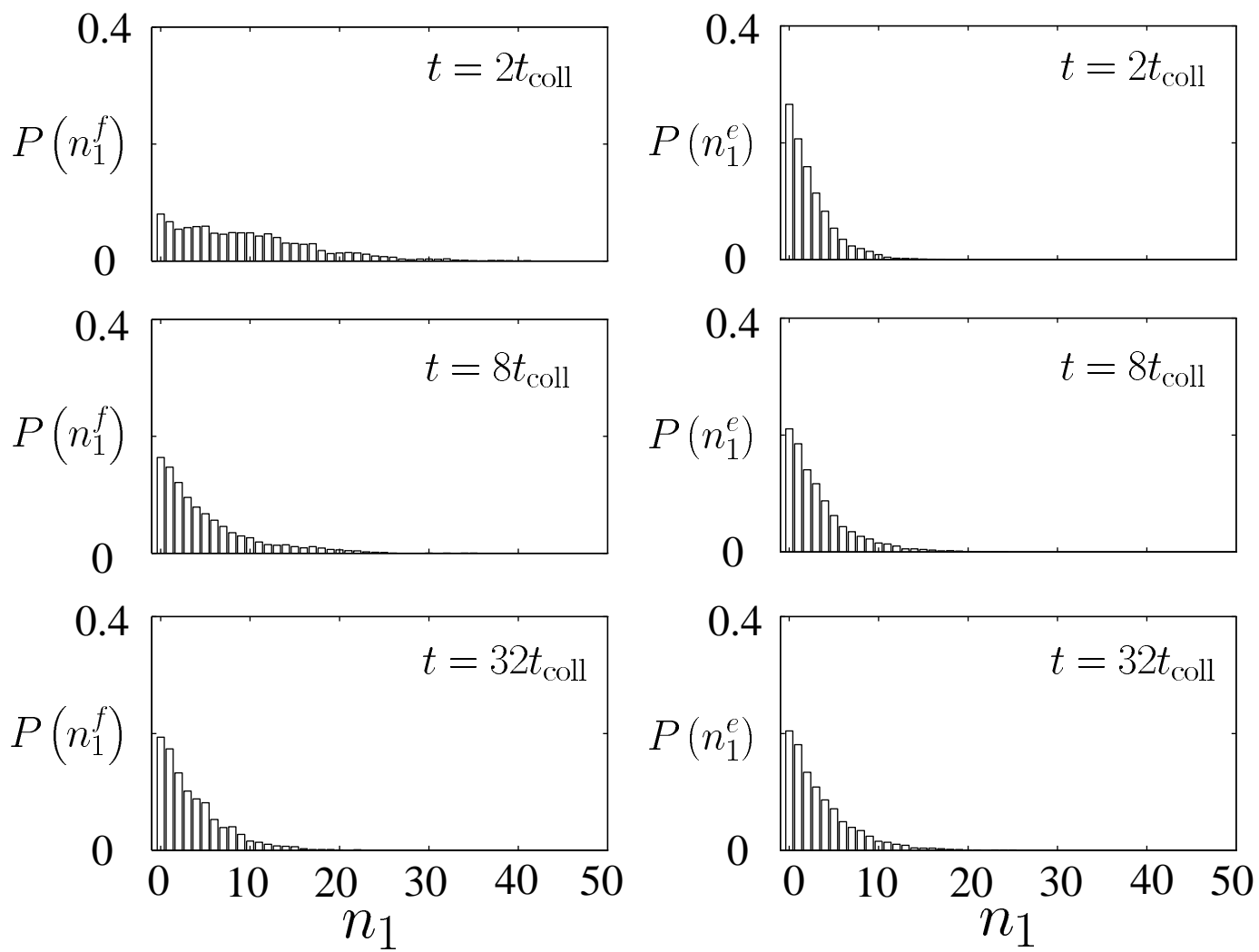


Fig. 10

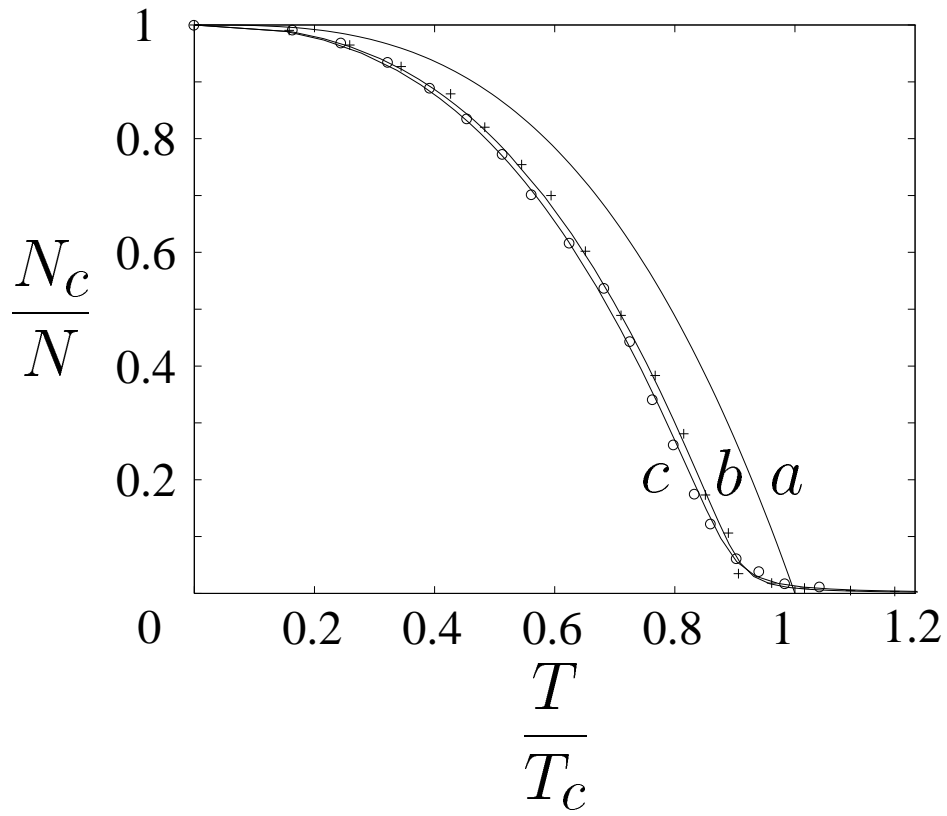


Fig. 11

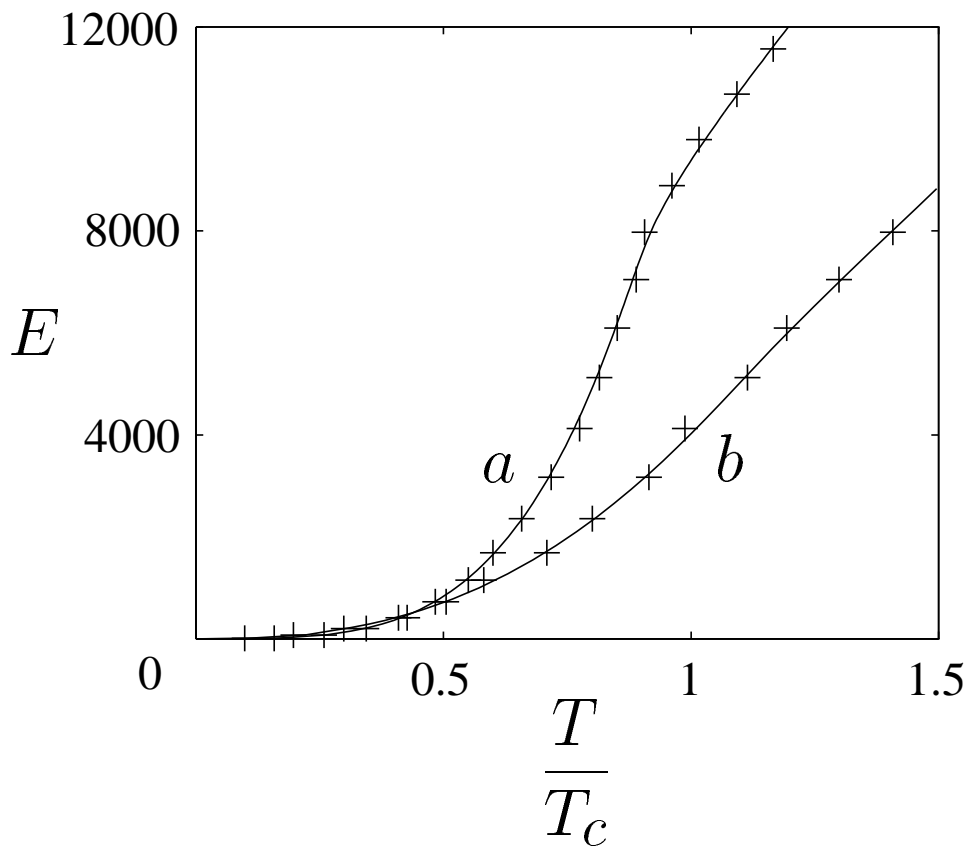


Fig. 12

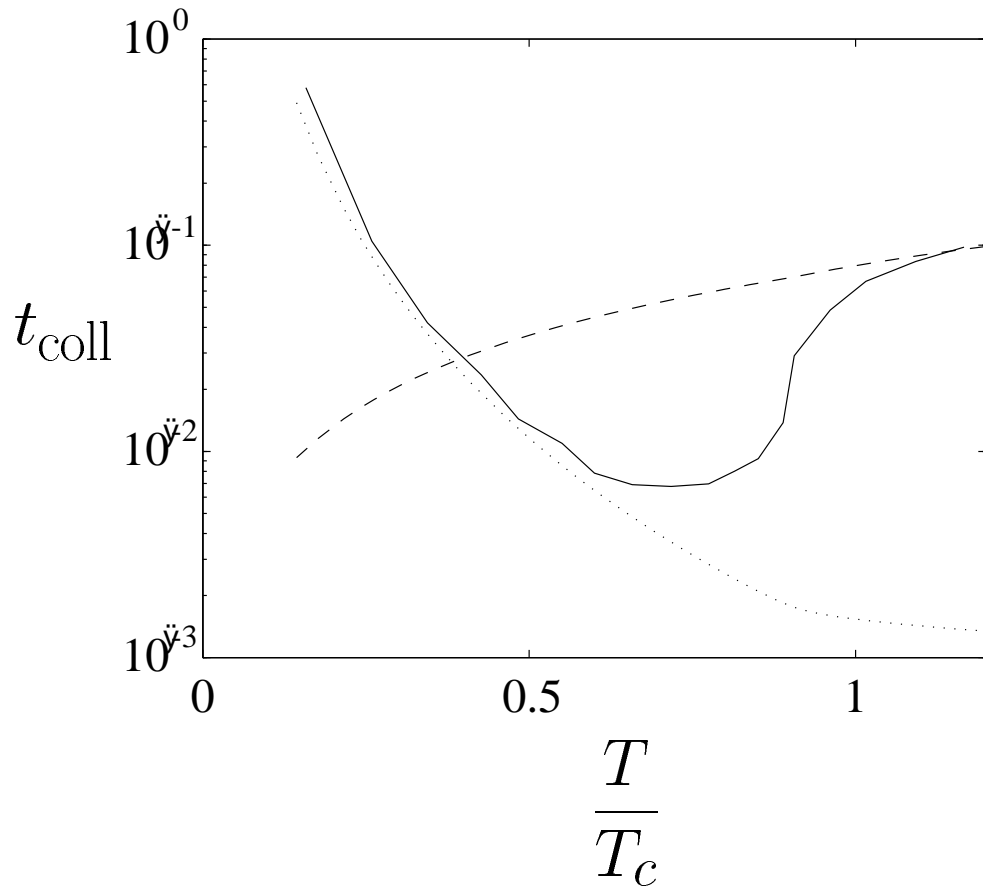


Fig. 13

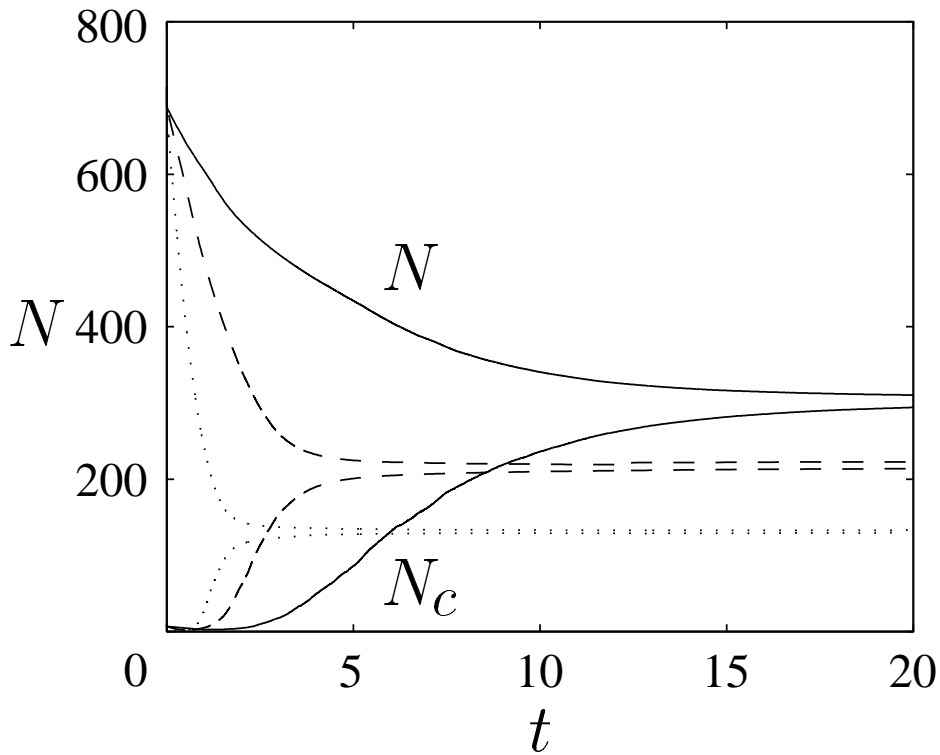


Fig. 14

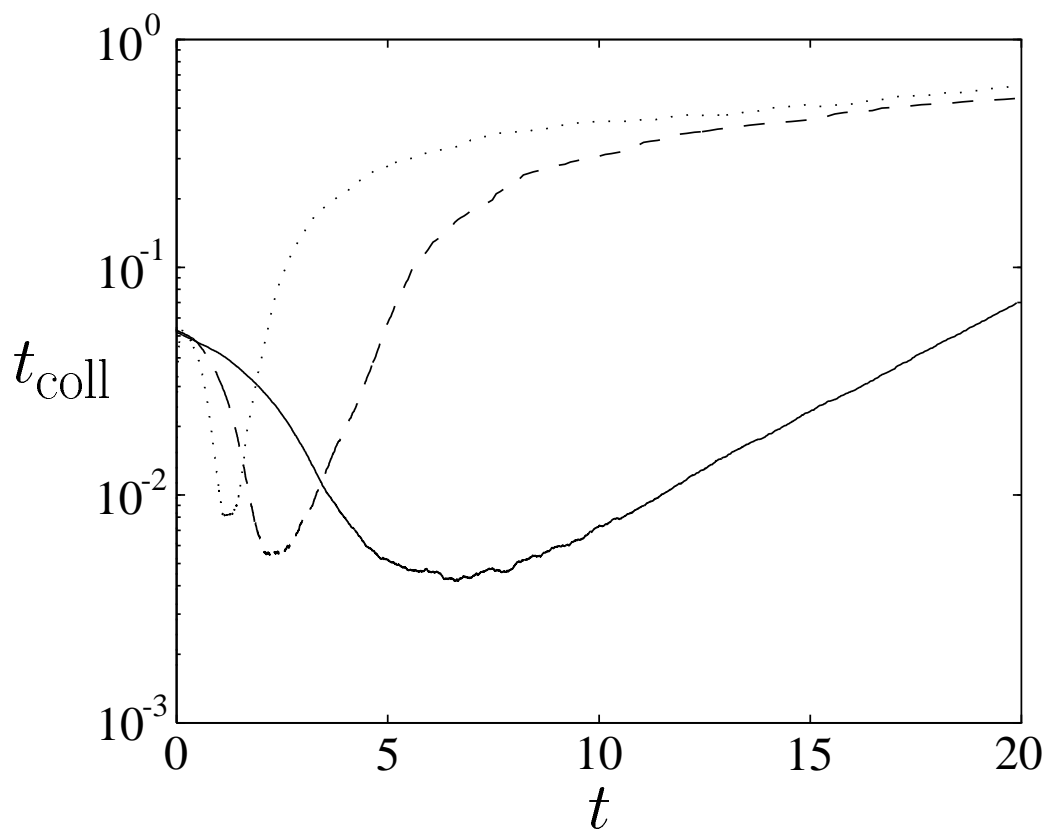


Fig. 15

